Accepted Manuscript

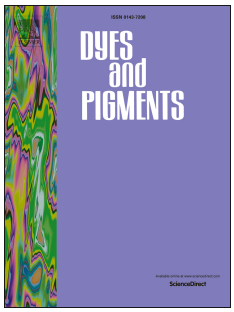

Synthesis, experimental and theoretical photophysical study of proton transfer based oxazoline fluorophores. Potential tailor made optical sensors for enantiomeric detection in solution

Fabiano S. Santos, Gabriel M. Zanotto, Luis M.Z. Argomedo, Mariana P. Darbem, Paulo F.B. Gonçalves, Helio A. Stefani, Fabiano S. Rodembusch

PII: S0143-7208(19)30019-1

DOI: https://doi.org/10.1016/j.dyepig.2019.02.047

Reference: DYPI 7381

To appear in: *Dyes and Pigments*

Received Date: 3 January 2019

Revised Date: 11 February 2019

Accepted Date: 25 February 2019

Please cite this article as: Santos FS, Zanotto GM, Argomedo LMZ, Darbem MP, Gonçalves PFB, Stefani HA, Rodembusch FS, Synthesis, experimental and theoretical photophysical study of proton transfer based oxazoline fluorophores. Potential tailor made optical sensors for enantiomeric detection in solution, *Dyes and Pigments* (2019), doi: https://doi.org/10.1016/j.dyepig.2019.02.047.

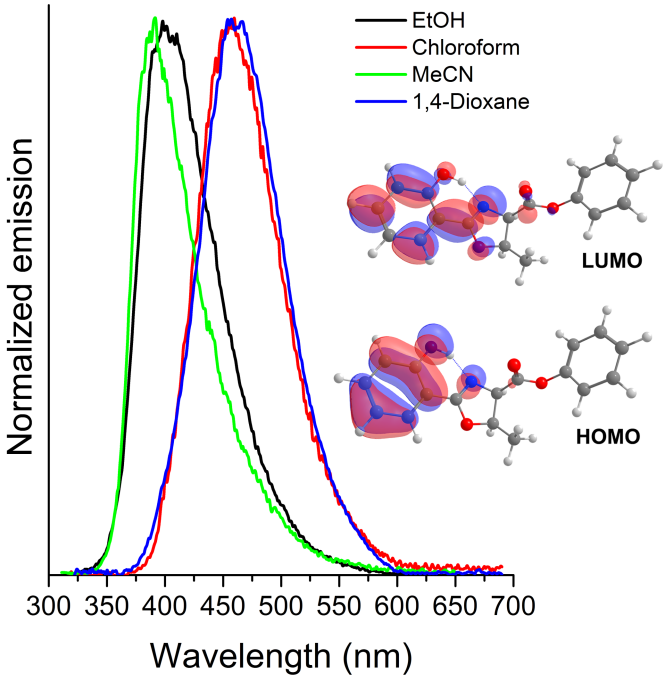

Synthesis, experimental and theoretical photophysical study of proton transfer based oxazoline fluorophores. Potential tailor made optical sensors for enantiomeric detection in solution

Fabiano S. Santos,[a] Gabriel M. Zanotto,[b] Luis M. Z. Argomedo,[c] Mariana P. Darbem,[c] Paulo F. B. Gonçalves,[b] Helio A. Stefani,[c,*] Fabiano S. Rodembusch[a,*]

[a]Grupo de Pesquisa em Fotoquímica Orgânica Aplicada, Universidade Federal do Rio Grande do Sul – Instituto de Química, Av. Bento Gonçalves 9500, CEP 91501-970 Porto Alegre, RS, Brazil. Fax: +55 51 3308 7304; Tel: +55 51 3308 7204. E-mail: rodembusch@iq.ufrgs.br

[b]Grupo de Química Teórica, Universidade Federal do Rio Grande do Sul – Instituto de Química, Av. Bento Gonçalves 9500, CEP 91501-970, Porto Alegre, RS, Brazil. E-mail: paulo@iq.ufrgs.br

[c]Universidade de São Paulo, Faculdade de Ciências Farmacêuticas, Av. Prof. Lineu Prestes 580 - Bloco 13 Superior, Cidade Universitária, CEP 05508-900, São Paulo, SP, Brazil. E-mail: hstefani@usp.br

Keywords: oxazoline, proton transfer, optical sensor, enantiomeric sensing, ESIPT

Abstract

A series of oxazoline based compounds was obtained via amidation formation from salicylic acid derivatives and benzyl-protected L-threonine with good yields (50-90%). These compounds present absorption in the UV region (~300 nm) and fluorescence emission spectra show large Stokes shift emission (~10000 cm^{-1}) in the blue-green region attributed to the ESIPT process. TD-DFT calculations were carried out to investigate the process of proton transfer of the structure of both tautomers (keto and enol) and corroborating the UV region absorption and large Stokes shift. The oxazolines derivatives were investigated as optical sensor for enantiomeric identification in solution. Preliminary results indicate sensing for arabinose and tartaric acid, but not specificity. However, to

the pair R-(-)-Mandelic and S-(+)-Mandelic acid, the oxazoline **4c** showed a enantiomeric seletivity identification, allowing to envisage these compounds as potential photoactive building blocks to propose innovative optical sensors in solution.

1. Introduction

Oxazoline is a five-membered heterocyclic compound containing one oxygen atom and one nitrogen atom. It was first characterized in 1889 and was named according to the nomenclature of Hantzsch-Widman [1]. The oxazoline ring itself has no applications, however, ring-containing compounds, present a wide variety of uses, sucha as synthetic intermediates [2-4], protector groups [5-7], binders [8], antioxidants [9-11], as well as chiral auxiliaries [12-14] in many organic transformations. Moreover, the oxazoline moiety can also be found in a number of compounds with applications in gasoline additives, protective films, photographic materials, fluorescent molecular probes and agrochemicals [2-4,15-24]. This broad use can be justified by resistance to several nucleophiles, free radicals, oxidizing agents and various acids, which facilitates their production through different synthetic routes, which can lead to highly complex compounds [15-21,25]. Oxazolines are central structures of many biologically active molecules, which exhibit cytotoxic [15], anti-bacterial [16] anti-tumor [17], antidepressant [19] and anti-Alzheimer activities [21]. In view of the structural viability offered by the nucleus and the possibility of the extension of π-conjugated systems, oxazolines are very promising building blocks due to their coordination properties, in the preparation of fluorescent markers in the detection of metallic elements, aiming at the identification of analytes of biological, technological or environmental interest [2-4,15-21,26-28].

Thus, the synthesis of molecules which exhibit remarkable photophysical properties, such as high photostability, solid state emission, almost absent inner filter effect due to large Stokes' shift are of great interest [29-36].

In this context, the literature has presented several structures based on flavonoid and benzazolic cores that present these properties due to a phototautomerism in the excited state [37]. However, compounds based on oxazolinic and chiral nuclei that exhibit these properties are poorly reported [38].

The phototautomerism in the excited state, so-called excited state intramolecular proton transfer (ESIPT) is a reversible photochemical process that produces a tautomeric specie from conformer present in the ground state (Figure 1) [39]. Generally, chemical structures which present intramolecular hydrogen bond (IHB) between the H atom of the donor group and the acceptor within a distance less than 2Å are able to proton transfer in the excited state [40]. The observed electronic redistribution in the excited state takes place between a donor moiety, usually a phenol or aniline groups and an acceptor group (imino/azonitrogen- or carbonyl-oxygen-containing ring skeleton), which are more acidic and basic after radiation absorption, respectively [41].

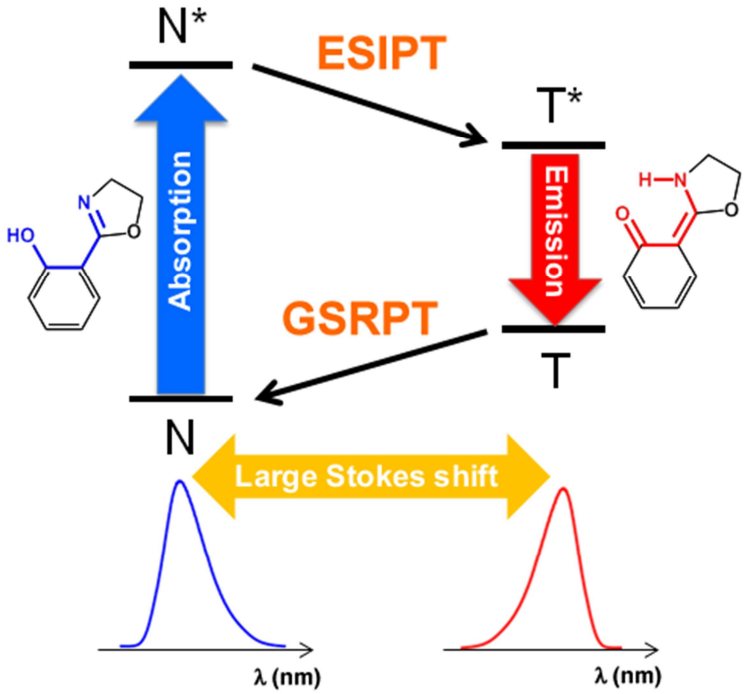

Figure 1. ESIPT process for a generic oxazolinic core, where N and T are the normal and tautomeric species, respectively and GSRPT is the ground state retro proton transfer. The asterisk indicates the excited state.

2. Experimental

2.1. Materials and methods

UV-Vis absorption spectra in solution were performedon a Shimadzu UV-2450 spectrophotometer at a concentration range of 10^{-5}M. Steady state fluorescence spectra were taken using a Shimadzu spectrofluorometer RF-5301PC. The maxima absorption wavelengths were used as the excitation wavelengths for fluorescence measurements. Spectrum correction was performed to enable a

true spectrum to be recorded by eliminating instrumental responses such as wavelength characteristics of the monochromator or the detector using Rhodamine B as a standard. The quantum yield of fluorescence (Φ_{FL}) was measured at 25^{o}C using spectroscopic grade solvents within solutions applying the optical dilute methodology and Quinine sulfate (Riedel) in H_2SO_4 (1 N) as the quantum yield standard (Φ_{FL}=0.55) [42]. Time resolved fluorescence curves were performed in 1,4-dioxane and acetonitrile with an EasyLife V spectrophotometer (Optical Building Blocks). All measurements were performed at room temperature. The decay curves were analysed using EasyLife V software (OBB). A nonlinear least square method was employed for the fit of the decay to a sum of exponentials. The value of χ^2, respective residuals and the autocorrelation function were used to determine the quality of the proposed fit. To the enantiomer interaction study, in a solution of **4a-d** 10^{-5} M in acetonitrile different amounts of DMSO stock solutions 10^{-3} M of D-(-)-arabinose, L-(+)-arabinose, D-Tartaric acid, L-Tartaric acid, R-Mandelic acid or S-Mandelic acid were added. To this study a control experiment was performed using the achiral carboxilic benzoic acid (BA), where the oxazolines were measured in absence and in presence of BA at a molar ratio 1:1 sensor:analyte. The enantiomer and dye work concentrations are in ESI. All photophysical characterization was performed at 25^{o}C.

2.2. Synthesis

*General procedure for the synthesis of (2S,3R)-benzyl 3-hydroxy-2-(2-hydroxybenzamido)butanoate derivates (**3a-d**).*

2-hydroxybenzoic acid derivatives (**1a-d**) (1 mmol, 1 equiv) and benzyl threonine (1 mmol, 1 equiv), EDC·HCl (1-ethyl-3-(3-dimethylaminopropyl)carbodiimide (1.3 mmol, 1.3 equiv), 1-HOBt (1-hydroxybenzotriazole) (1.2 mmol, 1.2 equiv), N-methylmorpholine (1.5 mmol, 1.5 equiv) were dissolved in 5 mL of CH_2Cl_2. The reaction mixture was stirred for the required time at room temperature in ultrasonic bath. The completion of the reaction was monitored by thin layer chromatography (TLC). Then the reaction mixture was diluted with ethyl acetate and washed with saturated solution of NH_4Cl (3 × 20 mL), the organic phase was collected, dried over

$MgSO_4$, filtered and the solvent was removed under vacuum. The crude residue was purified by flash chromatography on silica gel (eluting with ethyl acetate/hexane 3:7).

*(2S,3R)-benzyl 3-hydroxy-2-(2-hydroxybenzamido)butanoate (**3a**)*

^{1}H NMR (300 MHz, $CDCl_3$) δ 11.99 (s, 1H), 7.55 (d, *J* = 7.9 Hz, 1H), 7.39 (d, *J* = 8.0 Hz, 6H), 7.02 (d, *J* = 8.3 Hz, 1H), 6.89 (t, *J* = 7.6 Hz, 1H), 5.35 – 5.16 (m, 2H), 4.85 (d, *J* = 10.7 Hz, 1H), 4.50 (s, 1H), 1.30 (d, *J* = 6.5 Hz, 3H). ^{13}C NMR (75 MHz, $CDCl_3$) δ 170.65, 170.39, 161.58, 135.09, 134.65, 128.70, 128.23, 125.95, 118.85, 118.56, 113.84, 68.11, 67.62, 57.16, 20.17. HRMS-ESI: calcd. for $C_{18}H_{19}NO_5$ [M+H$^+$]: 329,1263, found: 328,0800

*(2S,3R)-Benzil 2-(4-azido-2-hidroxibenzamido)-3-hidroxibutanoato (**3b**)*

RMN ^{1}H (300 MHz, $CDCl_3$) δ 11,69 (s, 1H); 7,36 (s, 5H); 7,26 (dd, *J* = 8,0, 3,5 Hz, 1H); 7,17 – 7,12 (m, 1H); 6,94 (dd, *J* = 9,1, 4,7 Hz, 1H); 5,24 (d, *J* = 5,4 Hz, 2H); 4,81 (d, *J* = 8,7 Hz, 1H); 4,49 (d, *J* = 5,1 Hz, 1H); 1,27 (d, *J* = 6,4 Hz, 3H). RMN ^{13}C (75 MHz, $CDCl_3$-*d*) δ 170,62; 169,28; 160,56; 137,35; 128,74; 128,69; 128,58; 128,29; 120,46; 115,3; 110,44; 68,06; 67,81; 57,27; 20,23. HRMS-ESI: calcd. for $C_{18}H_{18}N_4O_5$ [M+H$^+$]: 370,11277, found: 371,1760.

*(2S,3R)-benzyl 3-hydroxy-2-(2-hydroxy-5-methoxybenzamido)butanoate (**3c**)*

^{1}H NMR (300 MHz, $CDCl_3$) δ 7.38 (s, 4H), 7.15 (d, *J* = 7.1 Hz, 1H), 7.06 (d, *J* = 8.4 Hz, 2H), 6.95 (d, *J* = 8.6 Hz, 1H), 5.45 – 5.14 (m, 2H), 4.85 (d, *J* = 8.6 Hz, 1H), 4.64 – 4.37 (m, 1H), 3.78 (s, 3H), 1.29 (d, *J* = 6.4 Hz, 3H). ^{13}C NMR (75 MHz, $CDCl_3$) δ 170.68, 170.09, 155.60, 151.93, 135.09, 128.69, 128.59, 128.23, 121.53, 119.26, 113.74, 110.30, 68.12, 67.64, 57.26, 56.11, 20.18. HRMS-ESI: calcd. for $C_{19}H_{21}NO_6$ [M+H$^+$]: 359,1369, found: 360,1760.

*(2S,3R)-benzyl 3-hydroxy-2-(2-hydroxy-6-methoxybenzamido)butanoate (**3d**)*

^{1}H NMR (300 MHz, $CDCl_3$) δ 9.15 (d, *J* = 6.9 Hz, 1H), 7.65 – 6.99 (m, 6H), 6.63 (d, *J* = 8.4 Hz, 1H), 6.41 (d, *J* = 8.3 Hz, 1H), 5.24 (s, 2H), 4.82 (d, *J* = 8.1 Hz, 1H), 4.43 (s, 1H), 3.91 (d, *J* = 2.0 Hz, 3H), 1.27 (d, *J* = 6.4 Hz, 3H). ^{13}C NMR (75 MHz, $CDCl_3$-*d*) δ 170.69, 164.41, 159.00, 133.75, 128.67, 128.52, 128.21,

111.68, 103.71, 101.18, 68.15, 67.41, 57.50, 56.36, 20.14. HRMS-ESI: calcd. for $C_{19}H_{21}NO_6$ [M+H$^+$]: 359,1369, found: 360,1730.

*General procedure for the synthesis (4S,5S)-benzyl 2-(2-hydroxyphenyl)-5-methyl-4,5-dihydrooxazole-4-carboxylate derivates (**4a-d**).*

Thionyl chloride (30 mmol, 30 equiv) was added dropwise to the compound 3 (1 mmol, 1 equiv) dissolved in dichloromethane (10 mL) under nitrogen atmosphere. The reaction mixture was stirred at room temperature for 24 h. Then Na_2CO_3 was added until the solution turned basic. The inorganic solid was filtered off, and organic phase was concentrated under vacuum. The crude product was purified by flash chromatography on silica gel (eluting with ethyl acetate/hexane 1:9).

*(4S,5S)-benzyl 2-(2-hydroxyphenyl)-5-methyl-4,5-dihydrooxazole-4-carboxylate (**4a**)*

^{1}H NMR (300 MHz, $CDCl_3$) δ 11.85 (s, 1H), 7.68 (d, *J* = 6.5 Hz, 1H), 7.41 (s, 6H), 7.06 (d, *J* = 7.9 Hz, 1H), 6.90 (s, 1H), 5.26 (s, 2H), 5.07 (s, 2H), 1.38 (s, 3H). ^{13}C NMR (75 MHz, $CDCl_3$) δ 169.04, 167.61, 160.20, 135.15, 133.89, 128.64, 128.58, 128.32, 118.62, 116.96, 110.24, 70.31, 67.13, 15.99. HRMS-ESI: calcd. for $C_{18}H_{17}NO_4$ [M+H$^+$]: 312.1236, found: 312.1018.

*(4S,5S)-benzyl-2-(4-azido-2-hydroxyphenyl)-5-methyl-4,5-dihydrooxazole-4-carboxylate (**4b**)*

^{1}H NMR (300 MHz, $CDCl_3$) δ 7.40 (d, *J* = 8.5 Hz, 1H), 7.29 (s, 5H), 6.37 (s, 1H), 6.27 (d, *J* = 8.0 Hz, 1H), 5.14 (s, 2H), 4.91 (d, *J* = 2.6 Hz, 2H), 1.25 (d, *J* = 5.5 Hz, 3H). ^{13}C NMR (75 MHz, $CDCl_3$) δ 168.65, 166.59, 160.99, 159.80, 134.08, 128.89, 127.59, 106.18, 102.58, 102.04, 69.06, 66.20, 14.95. HRMS-ESI: calcd. for $C_{18}H_{16}N_4O_4$ [M+H$^+$]: 353.1250, found: 353.1003.

*(4S,5S)-benzyl 2-(2-hydroxy-5-methoxyphenyl)-5-methyl-4,5-dihydrooxazole-4-carboxylate (**4c**)*

^{1}H NMR (300 MHz, $CDCl_3$) δ 7.29 (s, 5H), 7.05 (s, 1H), 6.90 (d, *J* = 11.3 Hz, 2H), 5.30 – 5.08 (m, 2H), 4.95 (s, 2H), 3.69 (s, 3H), 1.27 (s, 3H). ^{13}C NMR (75 MHz, $CDCl_3$) δ 169.03, 167.46, 154.64, 151.83, 135.16, 128.59, 121.79,

117.89, 111.12, 109.75, 77.46, 70.43, 67.13, 55.94, 16.02. HRMS-ESI: calcd. for $C_{19}H_{19}NO_5$ [M+H$^+$]: 342.1341, found: 342.1099.

*(4S,5S)-benzyl 2-(2-hydroxy-6-methoxyphenyl)-5-methyl-4,5-dihydrooxazole-4-carboxylate (**4d**)*

^{1}H NMR (300 MHz, MeOD-d_4) δ 7.85 (d, *J* = 7.9 Hz, 1H), 7.42 – 7.27 (m, 6H), 6.67 (d, *J* = 8.1 Hz, 1H), 5.22 (s, 3H), 3.97 (s, 2H), 3.31 (s, 3H), 1.24 (d, *J* = 5.8 Hz, 3H). ^{13}C NMR (75 MHz, MeOD-d_4) δ 171.83, 168.12, 162.03, 143.33, 137.16, 129.58, 129.30, 129.14, 126.84, 105.37, 103.57, 101.40, 68.42, 68.21, 68.03, 59.49, 57.32, 20.78. HRMS-ESI: calcd. for $C_{19}H_{19}NO_5$ [M+H]$^+$: 342.1341, found: 342.1182.

2.4 Theoretical calculations

Theoretical calculations were performed using Gaussian 16 package [43]. Geometry optimizations of both enol and keto ground and excited states were carried out using ωB97XD, a hybrid functional which provides empirical dispersion and long-range correction [44]. The cc-pVDZ basis set [45] were used to all the geometry optimizations, while the electronic transition and energies calculations were carried out with *jun*-cc-pVTZ basis set [45]. This functional and basis functions has been used in previous works and have demonstrated good outcomes [46]. In order to account for solvent effects the Polarizable Continuum Model (PCM) [47] was applied to all DFT and TDDFT calculations for three different solvents: 1,4-dioxane, acetonitrile and dimethylsulfoxide. All the structures and frontier orbitals images were renderized using the graphical software CHEMCRAFT [48].

3. Results and Discussion

3.1 Synthesis

The synthesis of the oxazoline compounds was initiated via amidation formation step [49], starting with the derivatives of the salicylic acid (**1a-d**) and benzyl-protected *L*-threonine (**2**), which was obtained by refluxing L-threonine with benzyl alcohol [50] as shown in Scheme 1.

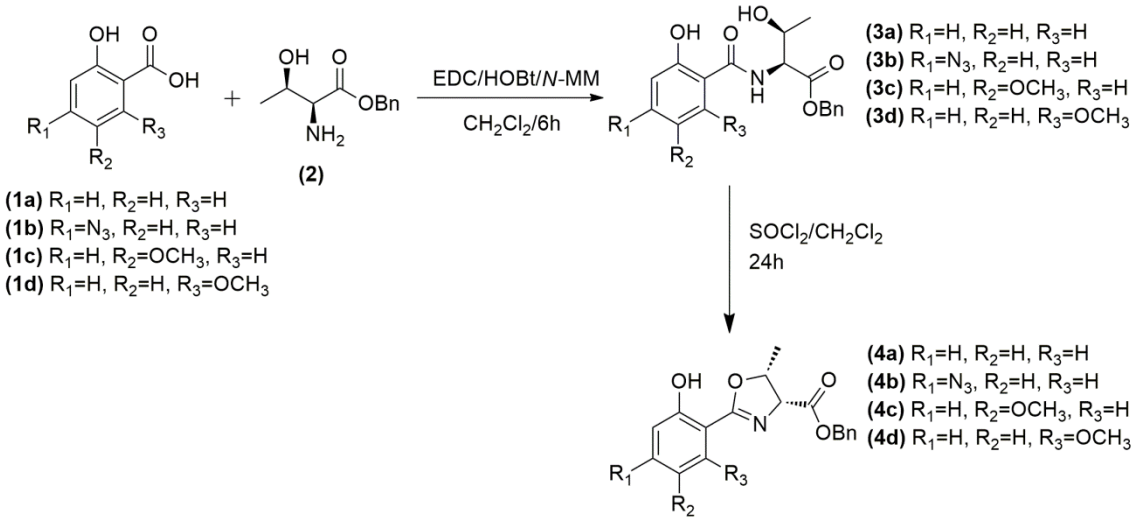

Scheme 1. Synthetic route for the 2-ariloxazolines (**4a-d**) derived from salicylic acid derivatives (**1a-d**).

The amidation formation was achieved using non-protected salicylic acid derivatives **1a-d**, benzyl threonine, 1.3 eq of EDC (1-ethyl-3-(3-dimethylaminopropyl)carbodiimide), 1.2 eq. of 1-HOBt (1-hydroxybenzotriazole), and 1.5 eq. of base in dichloromethane as solvent, leading to the coupling products **3a-d**, respectively with good yields (50-90%). This synthetic protocol was optimized employing an ultrasonic bath [51], which reduced significantly the reaction time to about 1h, in comparison with 12h for “on bench” synthesis [52]. In the next step to obtain the corresponding oxazolines **4a-d**, thionyl chloride (30 mmol, 30 equiv) was added dropwise to the compounds **3a-d** (1 mmol, 1 equiv) dissolved in CH_2Cl_2 (10 mL) under nitrogen atmosphere. The reaction mixture was stirred at room temperature for 24 h. Then Na_2CO_3 was added until the solution turned basic.

3.2. Photophysical characterization

The absorption spectra of the oxazoline **4b** is shown in Figure 2. The relevant data calculated from UV-Vis absorption spectroscopy for all compounds are presented in Table 1. It can be observed an absorption maxima located around 300-334 nm. It was observed a small solvatochromic effect ($\Delta\lambda_{abs}$~2 nm) in these compound. It could be observed that in all studied solvents, the derivative **4c** present red shifted absorption in despite of the **4d**, indicating a better

electron delocalization in solution (Table 1). The observed blueshift values for the absorption maxima in the polar protic ethanol are probably due to specific solvent-fluorophore interaction, such as hydrogen bonding,[53] that was also observed in methanol and isopropyl alcohol (data not shown, see SI).

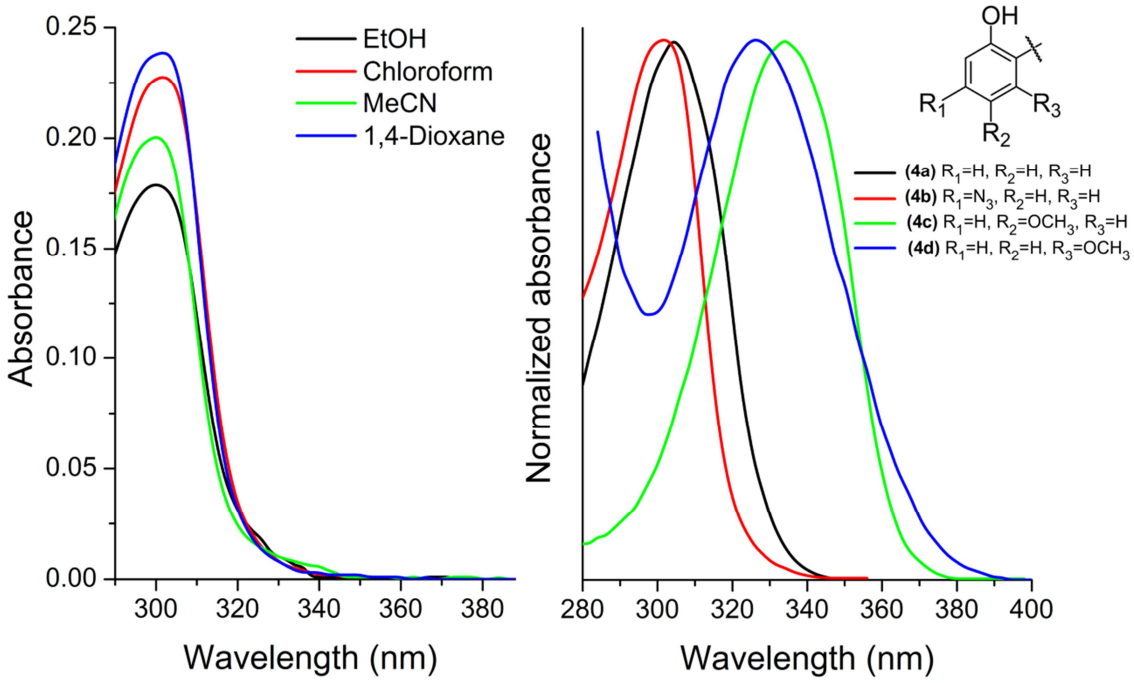

Figure 2. UV-Vis absorption spectra in solution (10^{-5} M) of oxazoline **4b** in different organic solvents (left) and oxazolines **4a-d** in chloroform (right). The inset presents the substitution pattern of the aromatic ring for comparison.

In order to discuss the photophysics in the ground state regarding the different contribution and position of the substituents, Figure 2b presents the UV-Vis spectra from **4a-d** in chloroform. It can be observed that changes in the substituent affect the absorption maxima due to different electronic contributions of these lateral groups. An absorption maxima between 302 nm and 334 nm were observed. Despite compound **4b** present a chromophoric group, this compound showed the shortest absorption maximum, located at 302 nm. This result probably indicates that the azido group does not contributes significantly to the conjugation of this compound [54]. On the other hand, the presence and position of the methoxy auxochrome seems to affect the absorption maxima location of these compounds. A redshift absorption is observed for compounds **4c** and **4d** (334 nm and 326 nm, respectively) in despite of **4a** and **4b**. In

addition, compound **4c** with the methoxy group at the 6-position presents the longer absorption wavelength probably due to electronic interaction with the hydroxyl group present in the para-position.

The UV-Vis absorption spectra also allow to calculate, using Eq. 1-3, the oscillator strength (f_e) and the radiative rate constant for emission (k_e^0), which is the probability of emission of photons per time unit, as well as the pure radiative lifetime (τ^0), applying the Strickler-Berg equation [55,56].

$$f_e = 4.32 \times 10^{-9} \int \varepsilon(\bar{\nu})\, d\bar{\nu}, \quad (1)$$

$$k_e^0 \approx 2.88x10^{-9} \bar{\nu}_0^2 \int \varepsilon(\bar{\nu}) d\bar{\nu}, \quad (2)$$

$$\tau^0 = 1/k_e^0, \quad (3)$$

where the integral is the area under the absorption curve, which corresponds to a single electron oscillator and $\bar{\nu}_0$ is the wavenumber corresponding to the maximum wavelength of absorption. The obtained molar absorptivity coefficient ε values (10^4 $M^{-1}\cdot cm^{-1}$) and the calculated radiative rate constant (10^7 s^{-1}) indicate spin and symmetry allowed $^1\pi\rightarrow\pi^*$ electronic transitions for **4a-d**, with typical range values to ε (10^2-10^6 $M^{-1}\cdot cm^{-1}$) and k_e^0 (10^5-10^9 s^{-1}). The values of the intrinsic property and independent of the electromagnetic field responsible for the excitation, the oscillator strength, ($f_e \approx 10^{-3}$-1) corroborates with electronic dipole-allowed transitions, as expected [57]. In addition, the calculated radiative lifetime (τ^0) values indicates that the oxazolines **4a-d** populate the same excited state.

Table 1. Relevant photophysical data of the UV-Vis absorption spectroscopy, where λ_{abs} is the absorption maxima (nm), ε is the molar absorptivity coefficient (10^4 $M^{-1}\cdot cm^{-1}$), f_e is the calculated oscillator strength, k_e^0 is the calculated radiative rate constant (10^7 s^{-1}) and τ^0 is the calculated pure radiative lifetime (in ns).

Dye	Solvent	λ_{abs}	ε	f_e	k°_e	τ°
4a	$CHCl_3$	306	4.80	0.08	8.19	12.2
	EtOH	304	4.63	0.08	8.21	12.2
	MeCN	304	3.81	0.06	6.63	15.1
	1,4-Dioxane	306	5.03	0.08	8.45	11.8
4b	$CHCl_3$	302	11.6	0.14	15.6	6.39
	EtOH	300	9.11	0.11	11.7	8.52
	MeCN	300	10.2	0.12	12.9	7.73
	1,4-Dioxane	301	12.2	0.15	16.4	6.10
4c	$CHCl_3$	334	5.76	0.10	8.79	11.4
	EtOH	332	5.76	0.10	9.48	10.5
	MeCN	332	4.92	0.09	7.91	12.6
	1,4-Dioxane	334	5.00	0.09	8.51	11.8
4d	$CHCl_3$	326	2.71	0.05	4.8	20.7
	EtOH	324	2.67	0.05	4.75	21.0
	MeCN	326	2.30	0.05	4.89	20.5
	1,4-Dioxane	324	2.67	0.05	4.98	20.1

The normalized fluorescence emission spectra of oxazolines **4a-d** are presented in Figure 3. The emission curves were obtained exciting the compounds at the absorption maxima wavelength and the relevant data from fluorescence emission spectroscopy is summarised in Table 2.

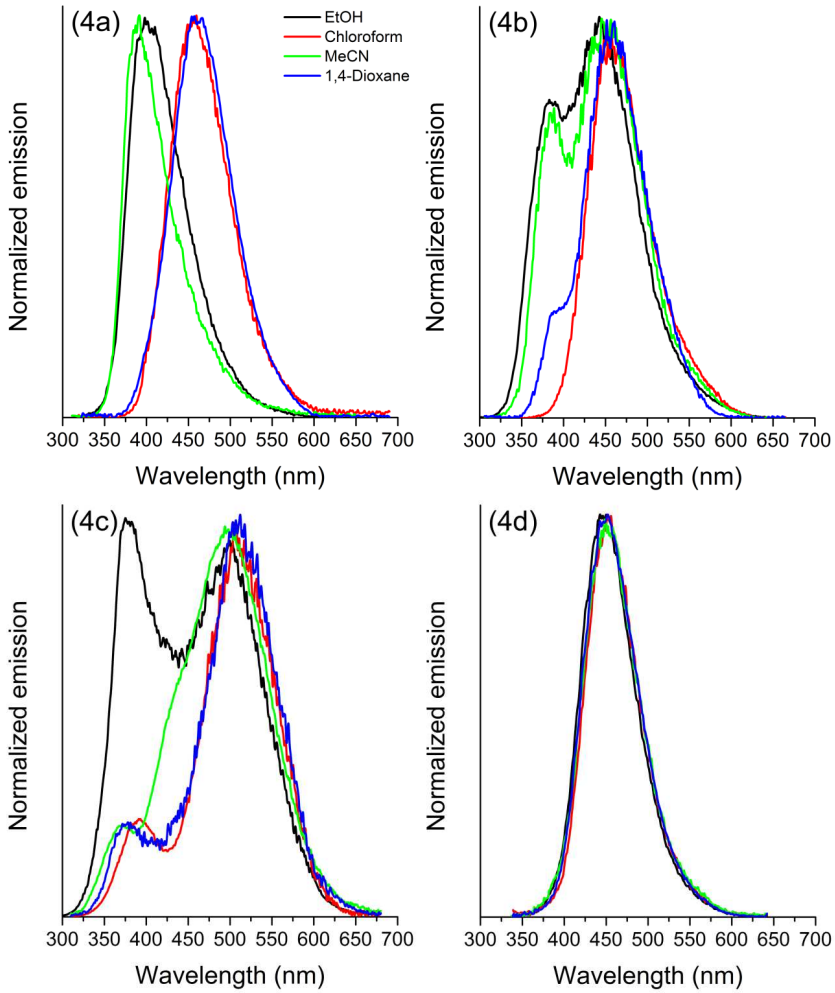

Figure 3. Steady-state normalized fluorescence emission spectra in solution (10^{-5} M) of the oxazolines **4a-d**.

It can be observed that these compounds do not present any clear tendency based on the substituents or the solvent polarity. However, all studied compounds present at least a longer wavelength emission, ascribed to the ESIPT process, indicating that the solvents stabilize the enol conformer that proton transfer in the excited state. In these compounds, after UV absorption, a locally excited enol-cis conformer (N*) tautomerizes to an excited-state keto (T*) specie, which decays to the ground state (T) emitting fluorescence at 442-510 nm with a large Stokes shift (~10000 cm^{-1}). It can also be observed that compounds **4a-c** present an additional blueshifted emission band, ascribed to a normal emission. In these compounds, after UV absorption, a non-ESIPT conformer (N*) decays emitting fluorescence at 369-400 nm. The ESIPT process requires the existence of an intramolecular hydrogen bond (IHB)

between the H atom of the donor group and the acceptor within a distance less than 2Å, as well as both photoacid and photobasic character [58,59]. In this way, the observed normal emission for the oxazolines **4a-c** indicates that a conformational equilibirium is present in the ground-state, as already observed in ESIPT compounds [60]. This equilibrium takes place between an enol conformer, which undergoes proton transfer in the excited state, so-called enol-cis, with additional conformers that do not favor intramolecular hydrogen (Figure 4). Thus, the dual fluorescence emission for **4a-c** can be related to a conformational equilibrium in solution in the ground state, with an emission at longer wavelengths ascribed to the excited keto tautomer, and the blue shifted one due to conformational forms which presents a normal relaxation. These results are interesting, because the observed dual fluorescence emission [37] can allow for their potential application as optical sensors for polarity, polar protic solvents either quiral identification. The total fluorescence quantum yield are 1.6-13%, as expected for ESIPT compounds [37].

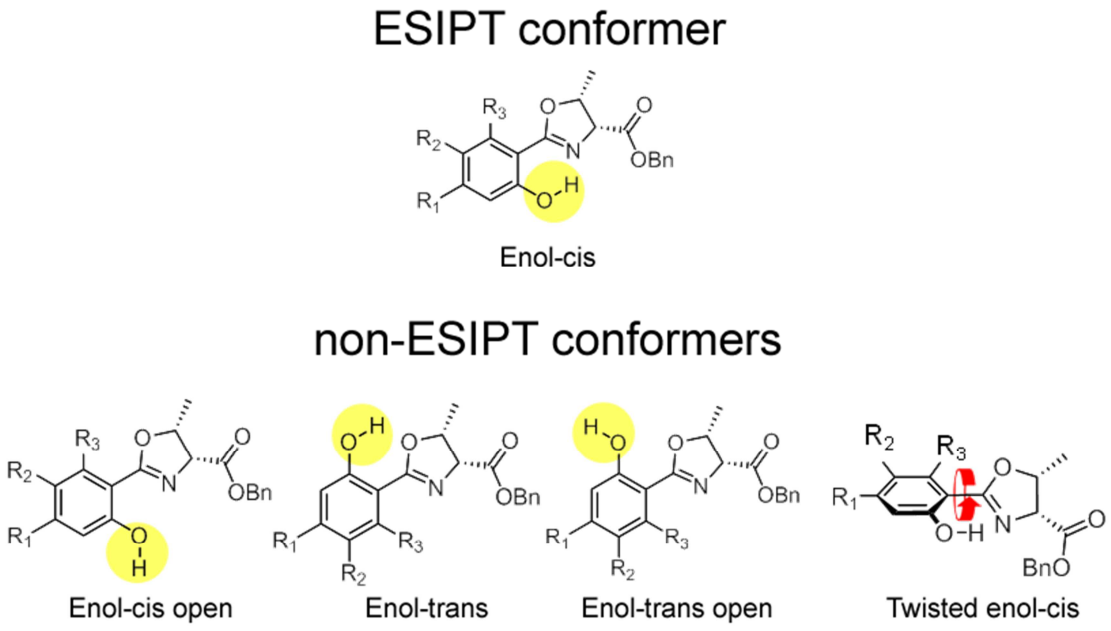

Figure 4. ESIPT (Enol-cis) and non-ESIPT conformers of the oxazoline studied in this work.

Table 2. Relevant photophysical data of the fluorescence emission spectroscopy, where λ_{em} is the emission maxima (nm) from the normal (N*) and tutomeric (T*) species, $\Delta\lambda_{ST}$ is the Stokes' shift (cm^{-1}) and Φ_F is the total fluorescence quantum yield (%).

Dye	Solvent	Normal		Tautomeric		Φ_F^*
		λ_{em}	$\Delta\lambda_{ST}$	λ_{em}	$\Delta\lambda_{ST}$	
4a	$CHCl_3$	-	-	457	10798	4.4
	EtOH	400	7895	-	-	6.9
	MeCN	391	7319	-	-	12.9
	1,4-Dioxane	-	-	462	11035	4.0
4b	$CHCl_3$	-	-	458	11279	4.7
	EtOH	385	7359	442	10709	2.0
	MeCN	386	7427	452	11209	4.0
	1,4-Dioxane	391	7647	460	11483	1.6
4c	$CHCl_3$	386	4033	507	10216	2.3
	EtOH	381	3874	500	10120	1.6
	MeCN	369	5903	498	10040	2.4
	1,4-Dioxane	380	6688	510	10332	1.2
4d	$CHCl_3$	-	-	452	8551	13.5
	EtOH	-	-	447	8493	6.2
	MeCN	-	-	452	8551	11.2
	1,4-Dioxane	-	-	448	8543	7.5

Time-resolved fluorescence was also employed to better understand the photophysics of these compounds (Figure 5). The relevant data are summarised in Table 3. The residuals are presented in the ESI.

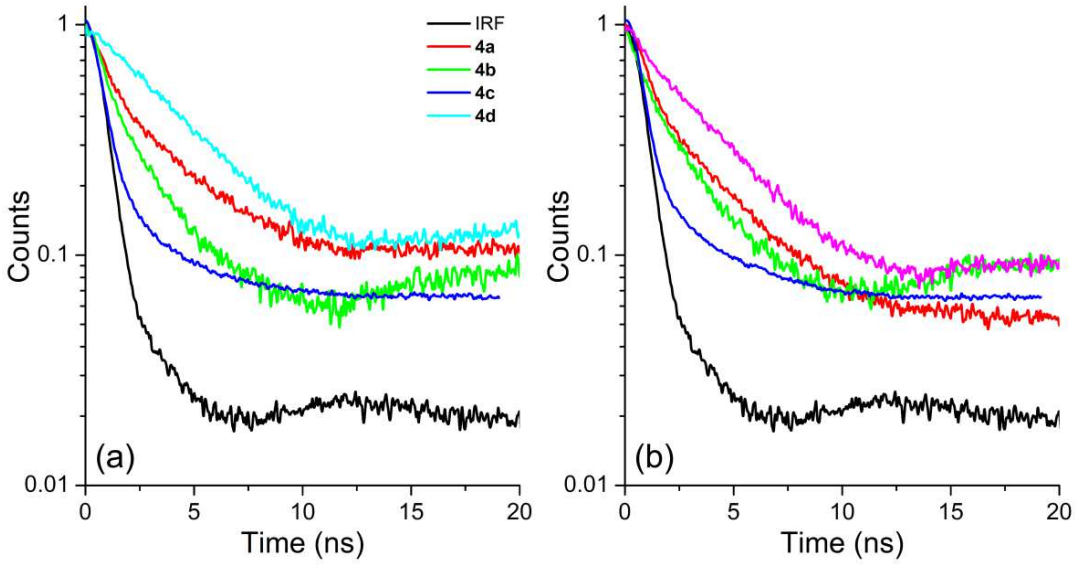

Figure 5. Fluorescence decays of oxazolines **4a-d** in (a) 1,4-dioxane and (b) acetonitrile [ca. 10^{-5} M]. IRF=instrument response factor.

The fluorescence decay profile of the oxazolines **4a-c** could be fitted by two-exponential decays both below 1 ns with good χ^2 values (Table 3). The individual time decays (τ_1 and τ_2), as well as the average lifetimes presented similar values ($\tau < 1$ ns) for these dyes. In addition, the solvent seems to present an almost absent influence on the decay profiles. Compound **4d** presented a quite particular behaviour, where one exponential decay was observed with a longer fluorescence lifetime (τ >3.4 ns) in both solvents. This latter corroborates with the previously calculated pure radiative lifetime (τ^0) presented in Table 1, indicating that somehow the substituent position plays a fundamental role on the dynamics of these compounds. Since **4d** this is the only derivative with a quite large substituent at the R_3 position (-OCH_3), it is believed that it is not only an electronic effect that is taking place in the excited state to allow such steady-state and time resolved photophysical behaviour. Probably sterically hindrance is also present to favor in this case, the enol-cis conformer, able to ESIPT in the excited state.

Table 3. Time resolved fluorescence spectroscopy of the oxazolines **4a-**c, where τ is the experimental fluorescence lifetime (in ns), τ_{av} is the weighted average fluorescence lifetime (in ns) and χ^2 determines the quality of the exponential fit. The numbers 1 and 2 are related to individual exponential decays.

Compound	Solvent	τ_1 (ns)	τ_2 (ns)	τ_{av} (ns)	χ^2
4a	MeCN	0.08 3 (96.59)	3.534 (3.41)	0.201	0.978
	1,4-Dioxane	0.414 (83.05)	3.640 (16.95)	0.961	0.974
4b	MeCN	0.192 (87.66)	2.239 (12.34)	0.445	0.967
	1,4-Dioxane	0.088 (95.72)	2.805 (4.28)	0.204	1.052
4c	MeCN	0.260 (96.91)	1.673 (3.09)	0.304	1.195
	1,4-Dioxane	0.459 (98.48)	4.958 (1.52)	0.528	1.139
4d	MeCN	3.476 (100)		3.476	1.151
	1,4-Dioxane	3.892 (100)		3.892	1.145

3.3. Enantiomers identification in solution

Based on the chiral structure, as well as their photophysical characteristics, the oxazolines **4a-d** were evaluated as optical sensors for enantioselective

detection of the follow optically active compounds: D-(-)-arabinose/L-(+)-arabinose, D-(-)-Tartaric acid/L-(+)-Tartaric acid and R-(-)-Mandelic acid/S-(+)-Mandelic acid. These compounds were chosen due to their different substituents, geometries and chemical groups. In this investigation, for all studied oxazoline it could be observed that their fundamental state was not differently affectec by one of the enantiomers of the pair, that is, quite similar shape and position were observed for the UV-Vis spectra of the oxazolines in presence of the enantiomers (data not shown, see SI). From the steady-state fluorescence spectra (Figure 6), it can be observed that the excited state of the oxazolines were notably affected by the presence of the enantiomers D-(-)-arabinose/L-(+)-arabinose and D-(-)-Tartaric acid/L-(+)-Tartaric acid. The oxazoline **4a** presents a main emission band locatd around 400 nm, which decreases its intensity and split into two emission bands in presence of the enantiomers, located at ~460 nm and ~375 nm. The emission at longer wavelentghs seems to keep constant during the enantiomer additon and the blue shifted emission bands presents a decrease on its intensity. The oxazoline **4b** in absence of the enantiomers already presents a dual fluorescence emission, which decreases upon addition of the enantiomers, indicating a significative interaction in the excited state between enantiomer and fluorophore, which can probably be related to the increase of the rigidity of the fluorophore and thus increasing its fluorescence quantum yield. Similar results were observed for the other oxazolines in presence of these enantiomers (see SI). The observed similar response in presence of both enantiomers (D or L) indicated that these enantiomers present significant interaction with the respective oxazolines, but not selectively. However, in presence of the R-(-)-Mandelic acid/S-(+)-Mandelic acid the oxazoline **4c** presents interesting changes on the emission spectra, indicating selective interaction between the fluorophore and the respective enantiomer (Figure 7). The derivatives **4a-b** and **4d** do not presented such photophysical behaviour (see SI).

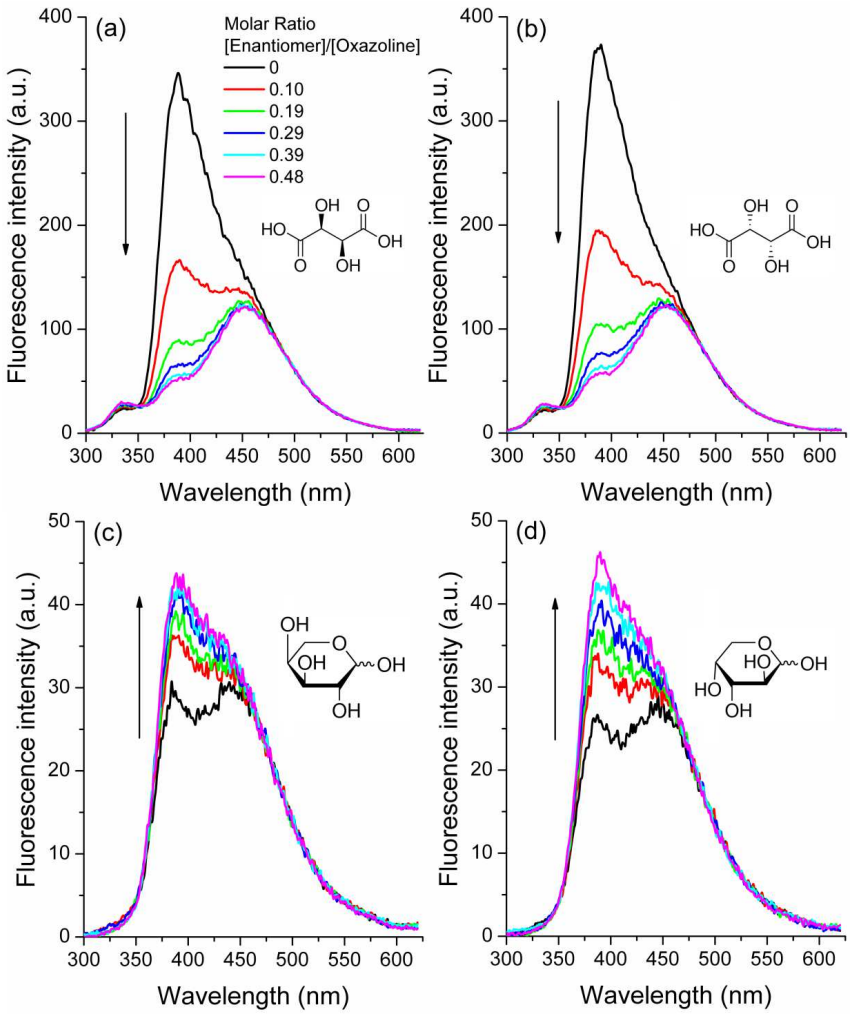

Figure 6. Fluorescence emission titration of oxazoline **4a** (10^{-5} M in DMSO) in diferents amounts of (a) D-(-)-Tartaric acid and (b) L-(+)-Tartaric acid and oxazoline **4b** (10^{-5} M in DMSO) in diferents amounts of (c) L-(+)-Arabinose and (d) D-(-)-Arabinose.

Despite the quite similar emission profile for **4c** in presence of R-(-)-Mandelic acid and S-(+)-Mandelic (λ_2 and λ_3 regions), it can be observed that at shorter wavelenghts, defined as λ_1, interesting changes were observed. In presence of the R-enantiomer, the fluorescence intensity below 400 nm changes slighlty if compared to the same region in presence of the S-enantiomer. It can be observed an increase of the fluorescence intensity upon addition of the S-enantiomer. Since this emission region can be related to non-ESIPT conformers, the observed increase on the emission instensity indicates that the S-enantiomer interacts with these species allowing their deactivation in despite of the enol-cis conformer, which would proton transfer in the excited state.

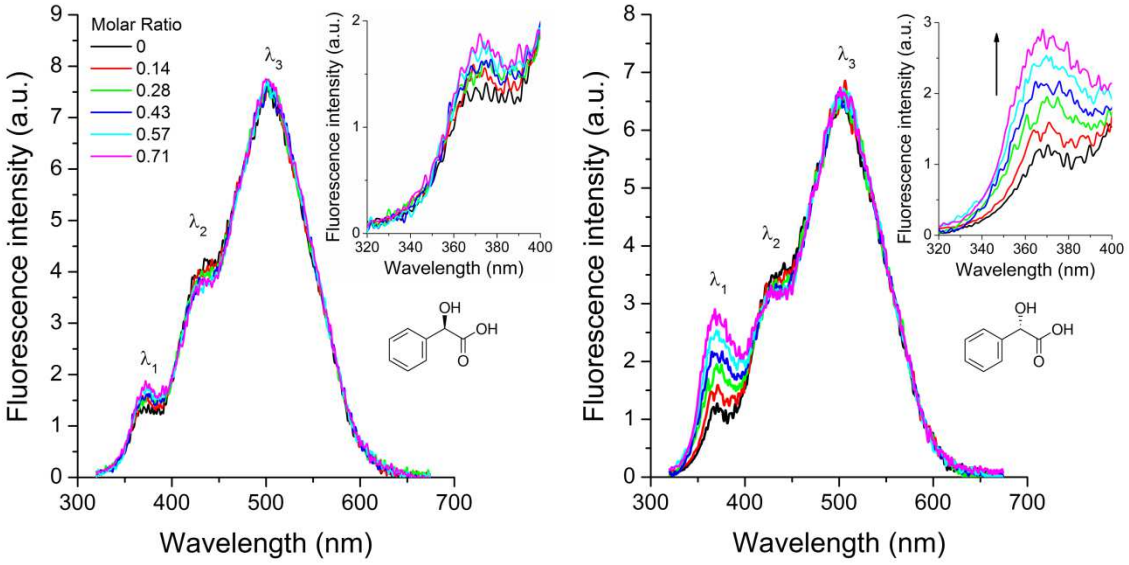

Figure 7. Fluorescence emission titration of oxazoline **4c** (10^{-5} M in DMSO) in diferents Molar Ratios [Mandelic Acid]/[Oxazoline] of (left) R-(-)-Mandelic acid and (right) S-(+)-Mandelic, where $\lambda_{1\text{-}3}$ are the respective emission bands. The inset presents the magnification of the λ_3 emission band.

These changes in intensity can be envisaged and clearly compared from fluorescence emission titration plots (Figure 8), where it can be observed that R-(-)-Mandelic and S-(+)-Mandelic acids present quite different behaviour. At the λ_1, the S-enantiomer presents a linear increase of the fluorescence intensity in relation to the enantiomer/oxazoline molar ratio if compared to the R-enantiomer. At the λ_2, both compounds present decrease on the intensity upon addition of the respective enantiomer. In addition, at λ_3 both compounds present a constant emission intensity. The observed photophysical features, although are not outstanding on-off or off-on fluorescence responses, which significantly restricts the application of fluorophores for enantiomers identification in solution are promising results. In addition, taking the control experiment into account, where benzoic acid (BA) was used as analyte, the almost absent changes on the UV-vis and fluorescence emission spectra of the oxazolines **4a-d** (see SI) even at a 1:1 (dye:BA) molar ratio corroborates with the potential application of these dyes for enantiomeric identification in solution.

It indicates that asymetrical fluorescent compounds even do not presenting specific chemical groups with their analytes can be applied as optical sensors, as recently reported in the literature [61].

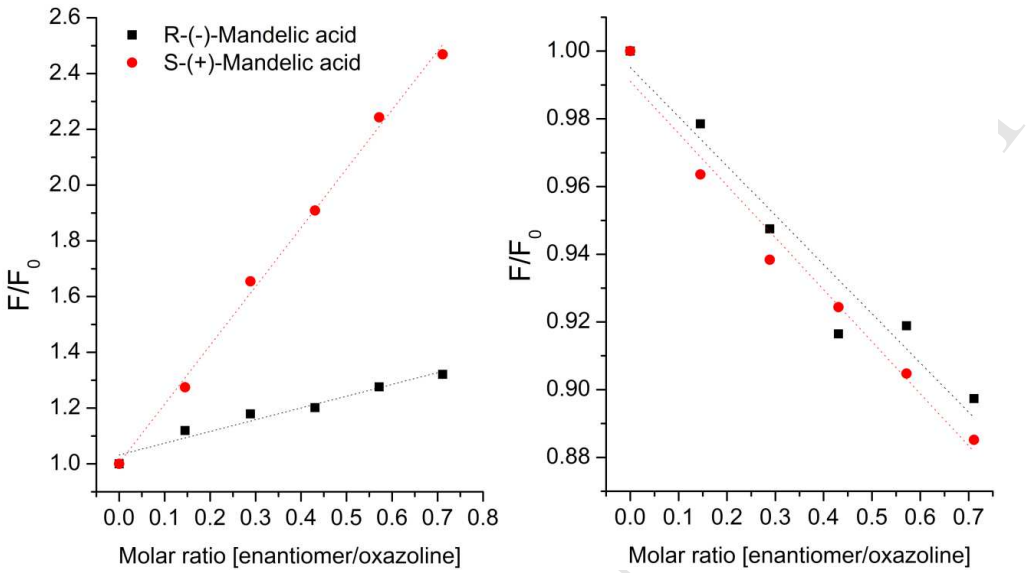

Figure 8. Ratio of the fluorescence emission intensities of oxazoline **4c** (10^{-5} M in DMSO) at diferents amounts of the enantiomers at (a) λ_1 and (b) λ_2.

3.4 Theoretical calculations

The **4a** and **4d** molecules were chosen for the TD-DFT study, since they are simple and representative structures of the studied compounds requiring minor computational effort. The computational protocol used indicates that for both molecules, the enol tautomer is the most stable in the ground state in all studied solvents as the keto tautomer showed to be less stable with respect to the enol conformer for both **4a** and **4d** molecules. Thus, the energy is absorbed by the enol conformer, as experimentally observed. Based on the enol and keto energies, it was decided to evaluate the absorption wavelengths only for the enol conformer, since it is the specie present in the ground state. It is worth mentioning that a similar analysis was carried out for the enol conformer and keto tautomer in the first excited state, resulting in the evaluation of the emission wavelengths only for the keto conformer. As expected, the geometry optimization for the enol tautomer in the first excited state led directly to the keto tautomer, indicating no energy barrier separating both tautomers. Figure 9

qualitatively illustrates the potential energy curves for the **4a** molecule. Compound **4d** presents the same energy curve profile.

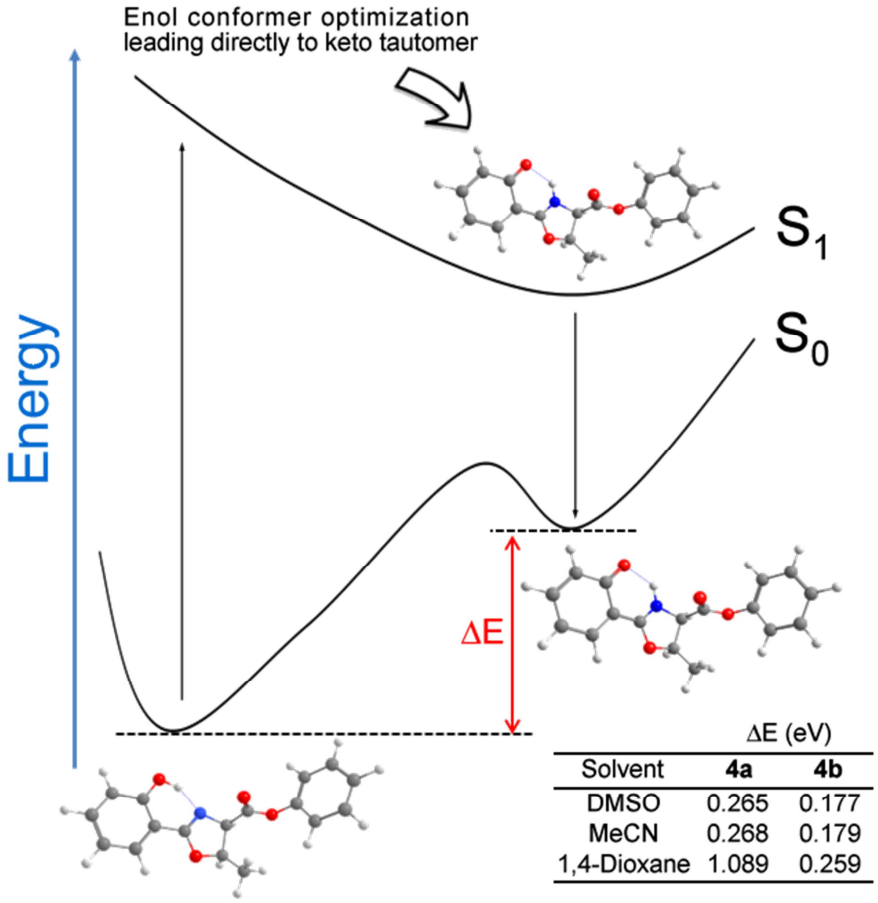

ΔE (eV)

Solvent	**4a**	**4b**
DMSO	0.265	0.177
MeCN	0.268	0.179
1,4-Dioxane	1.089	0.259

Figure 9. Potential energy curves of the ESIPT process for molecules **4a**, where Δe is the difference in energy from the conformers in the ground state.

The ESIPT is a well-known process where two species are involved: the enol conformer and the respective keto tautomer. In this sense, Figure 10 presents the optimized geometries of the predominant conformer to oxazolines **4a** and **4d** in dimethyl-sulfoxide in the ground and excited states. A similar behaviour was observed in acetonitrile and 1,4-dioxane (see SI).

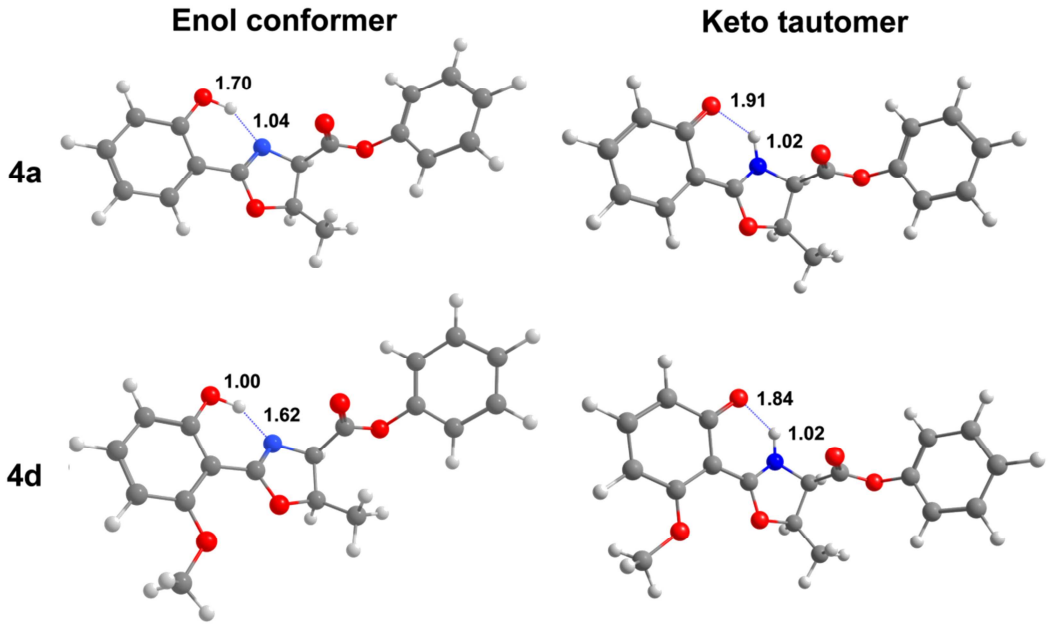

Figure 10. Enol (S_0) and keto (S_1) optimized geometries for oxazolines **4a** and **4d**, computed at the CAM-B3LYP/cc-pVDZ level in dimethylsulfoxide.

In Figure 11 it can be observed that the orbitals involved in the first electronic transition of compounds **4a** and **4d** in dimethylsulfoxide, indicate π-type orbitals for both oxazolines. Thus, it was assumed that π→π* transitions were occurring for both structures. In the ground state, the molecular ortbitals involved in the transition are almost exclusively localized at the phenolic ring. However, in the excited state, the orbitals have displaced towards the oxazolin ring, which is in agreement with the proton transfer process in these compounds. Once again, a similar behaviour was observed in acetonitrile and 1,4-dioxane (see SI).

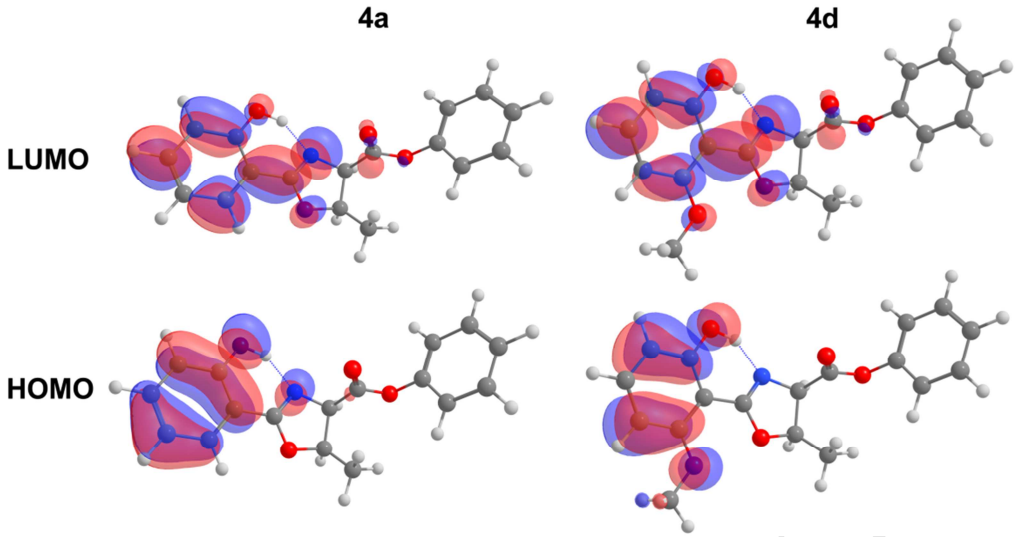

Figure 11. HOMO and LUMO for the first electronic transition of compounds **4a** and **4d**, computed at the CAM-B3LYP/jun-cc-pVTZ level in dimethylsulfoxide (DMSO).

The calculated photophysical data are shown in Table 4. The CAM-B3LYP/jun-cc-pVTZ absorption and emission wavelengths are in good agreement with the experimental data. Following the Förster cycle presented for the ESIPT process, the absorption wavelength were analyzed for the enol conformer and the emission wavelength for the keto tautomer. It could be observed that the overall deviation of the absorption and emission wavelengths, from the theoretical to the experimental data, is acceptable for the used protocol. Benchmark calculations shows that the chosen functional appropriate for electronic transitions analysis [62,63]. In addition, regarding the solvent effect, the calculations showed a small influence of solvent polarity on absorption and emision energies, in agreement with the experimental results.

It can also be observed that the theoretical Stokes shifts ($\Delta\lambda$) present values around 140 nm. Usually, large Stokes shifts are related to charge transfer (CT) processes, which in turn, are originated by large electronic displacement from the electron donor groups to acceptor groups. Charge transfer mechanism is also characterized by the great difference of the dipole moment between the ground and excited states, ($\Delta\mu$). However, based on the data presented in Table 4, the almost absent changes on the $\Delta\mu$ indicates that the ESIPT process

can be ascribed as the main responsible for the large Stokes shifts, as expected [64].

Table 4. Theoretical photophysical data for molecules **4a** and **4d,** where λ_{abs} is the absorption maxima (nm) for the enol conformer, λ_{em} is the emission maxima (nm) for the keto tautomer, *f* is the oscillator strength and μ is the dipole moment in Debye. The subscript 0 and 1 indicates the ground and excited states, respectively.

Dye	Solvent	enol			keto			Δλ	Δμ
		λ_{abs}	f_{abs}	μ_0	λ_{em}	f_{abs}	μ_1		
	1,4-Dioxane	276.83	0.19	4.69	417.44	0.19	3.87	140.61	0.82
4a	MeCN	273.55	0.18	5.68	413.43	0.27	6.20	139.88	-0.52
	DMSO	273.84	0.18	5.71	413.42	0.27	6.25	139.58	-0.54
	1,4-Dioxane	281.12	0.11	5.05	419.41	0.12	3.52	138.29	1.53
4d	MeCN	279.95	0.11	6.12	413.46	0.19	5.44	133.51	0.68
	DMSO	280.24	0.11	6.14	413.42	0.19	5.48	133.18	0.66

4. Conclusions

In summary, here we report the synthesis of new fluorescent proton-transfer dyes from non-trivial aromatic moieties. The oxazoline dyes were synthesized via amidation formation step with salicylic acid derivatives and benzyl-protected *L*-threonine with good yields. In a second step, thionyl chloride was used under nitrogen atmosphere to afford the desired products. The dyes presented absorption in the UV region and dual fluorescence emission located in the cyan-green with very large Stokes shift. Despite the absence of basic or acidic moieties in their chemical structure, the photophysical properties, as well as their chirality were used to explore these compounds for optical sensing in solution for enantioselective detection. For all studied oxazoline it could be observed that the enantiomers did not affectec the ground state of the oxazolines. On the other hand, the excited state of the oxazolines were notably affected by the presence of the enantiomers D-(-)-arabinose/L-(+)-arabinose and D-(-)-Tartaric acid/L-(+)-Tartaric acid. The observed similar response in presence of both enantiomers indicated that these enantiomers present

significant interaction with the respective oxazolines, but not selectively. However, in presence of the R-(-)-Mandelic acid/S-(+)-Mandelic acid the oxazoline **4c** presents interesting changes on the emission spectra, indicating selective interaction between the fluorophore and the respective enantiomer, which can be usefull to keep studying such structures for such application. The computational protocol applied to this study presented good agreement with the experimental findings in absorption and emission wavelengths

Acknowledgements

This work was supported by CNPq (fellowship 306119/2014-5 to HAS), Coordenação de Aperfeiçoamento de Pessoal de Nível Superior - Brasil (CAPES) - Finance Code 001, FAPERGS (17/2551-0000968-1) and FAPESP (grant # 2017/24821-4 and fellowship to MPD 2016/24396-9

5. References

[1] Gabriel S. Zur kenntniss des bromäthylamins. Ber Dtsch Chem Ges 1889;22:1139-1154.

[2] Gant TG, Meyers AI. The chemistry of 2-oxazolines (1985–present). Tetrahedron 1994;50:2297-2360.

[3] Reuman M, Meyers AI. The synthetic utility of oxazolines in aromatic substitution. Tetrahedron 1985;41:837-860.

[4] Frump JA. Oxazolines. Their preparation, reactions, and applications. Chem Rev 1971;71:483-505.

[5] Lee YJ, Lee J, Kim MJ, Jeong BS, Lee JH, Kim TS, Lee J, Ku JM, Jew SS, Park HG. Highly enantioselective synthesis of (2S)-alpha-(hydroxymethyl)-glutamic acid by the catalytic Michael addition of 2-naphthalen-1-yl-2-oxazoline-4-carboxylic acid tert-butyl ester. Org Lett 2005;7:3207-3209.

[6] Saravanan P, Corey EJ. A short, stereocontrolled, and practical synthesis of alpha-methylomuralide, a potent inhibitor of proteasome function. J Org Chem 2003;68:2760-2764.

[7] Greene TW, Wutz PGM. Protective groups in organic synthesis, 2nd ed. New York: John Wiley & Sons; 1991.

[8] Hargaden GC, Guiry PJ. Recent applications of oxazoline-containing ligands in asymmetric catalysis. Chem Rev 2009;109:2505-2550.

[9] Padmaja A, Rajasekhar C, Durgamma S, Venkatesh BC, Padmavathi V. Synthesis and antioxidant activity of pyrazolyl-oxazolines/thiazolines and isoxazolyl-oxazolines/thiazolines. Med Chem Res 2013;23:1084-1098.

[10] Djurendić E, Vujašković SD, Sakač M, Ajduković J, Gaković A, Kojić V, Bogdanović G, Klisurić O, Gaši KP. Synthesis and biological evaluation of some new 2-oxazoline and salicylic acid derivatives. Arkivoc 2011;2:83-102.

[11] Padmavathi V, Mahesh K, Dinneswara Reddy G, Padmaja A. Synthesis and bioassay of pyrrolyl oxazolines and thiazolines. Eur J Med Chem 2010;45:3178-3183.

[12] Khumsubdee S, Fan Y, Burgess K. A comparison between oxazoline-imidazolinylidene, -imidazolylidine, -benzimidazolylidene hydrogenation catalysts. J Org Chem 2013;78:9969-9974.

[13] McKeon SC, Müller-Bunz H, Guiry PJ. Synthesis of thiazoline-oxazoline ligands and their application in asymmetric catalysis. Eur J Org Chem 2011;35:7107-115.

[14] Sawada T, Nakada M. Asymmetric catalysis of intramolecular cyclopropanation of 5-aryl-1-diazo-1-mesitylsulfonyl-5-hexen-2-ones. Adv Synth Catal 2005;347:1527-532.

[15] Tsuda M, Yamakawa M, Oka S, Tanaka Y, Hoshino Y, Mikami Y, Sato A, Fujiwara H, Ohizumi Y, Kobayashi J. Brasilibactin A, a cytotoxic compound from actinomycete Nocardia brasiliensis. J Nat Prod 2005;68:462-464.

[16] Onishi HR, Pelak BA, Gerckens LS, Silver LL, Kahan FM, Chen M-H, et al. Antibacterial agents that inhibit Lipid A biosynthesis. Science 1996;274:980-982.

[17] Li Q, Woods KW, Claiborne A, Gwaltney II SL, Barr KJ, Liu G, Gehrke L, Credo RB, Hui YH, Lee J, Warner RB, Kovar P, Nukkala MA, Zielinski NA, Tahir SK, Fitzgerald M, Kim KH, Marsh K, Frost D, Ng SC, Rosenberg S, Sham HL. Synthesis and biological evaluation of 2-indolyloxazolines as a new class of Tubulin polymerization inhibitors. Discovery of A-289099 as an orally active antitumor agent. Bioorg Med Chem Lett 2002;12:465-469.

[18] Tsukamoto M, Murooka K, Nakajima S, Abe S, Suzuki H, Hirano K, Kondo H, Kojiri K, Suda H. BE-32030 A, B, C, D and E, New antitumor substances produced by Nocardia sp. A32030. J Antibiot 1997;50:815-21.

[19] Vizi ES. Compounds acting on alpha1- and alpha2- adrenoceptors: agonists and antagonists. Med Res Rev 1986;6:431-449.

[20] Celanire S, Talaga P, Leurs R, Denonne F, Timmerman H, Lebon F. Compounds comprising an oxazoline or thiazoline moiety, processes for making them, and their uses. US patent WO 2006103057 A1, 2006 Oct 05.

[21] Gross JL, Robichaud AJ, Mazzacani A, Williams MJ. Aminoalkylazole derivatives as histamine-3 antagonists. US patent US 0023707, 2009 Jan 22.

[22] Hoogenboom R. Poly(2-oxazoline)s: a polymer class with numerous potential applications. Angew Chem Int Ed 2009;48:7978-7994.

[23] Thijis L, Hanneke ML, Kuringen HPC, Put JPW, Schubert US, Hoogenboom R. Temperature induced solubility transitions of various poly(2-oxazoline)s in ethanol-water solvent mixtures. Polymers 2010;2:188-199.

[24] Li Y, Li C, Zheng Y, Wei X, Ma Q, Wei P, Liu Y, Qin Y, Yang N, Sun Y, Ling Y, Yang X, Wang Q. Design, synthesis, acaricidal activity, and mechanism of oxazoline derivatives containing an oxime ether moiety. J Agric Food Chem 2014;62:3064-3072.

[25] Meyers AI, Mihelich ED. The synthetic utility of 2-oxazolines. Angew Chem Int Ed 1976;15:270-281.

[26] Wu WH, Dong JJ, Wang X, Li J, Sui SH, Chen GY, Liu JW, Zhang M. Fluorogenic and chromogenic probe for rapid detection of a nerve agent simulant DCP. Analyst 2012;137:3224-3226.

[27] Dong XY, Si CD, Fan Y, Hu DC, Yao XQ, Yang YX, Liu JC. Effect of N-donor ligands and metal ions on the coordination polymers based on a semirigid carboxylic acid ligand: structures analysis, magnetic properties, and photoluminescence. Cryst Growth Des 2016;16:2062-2073.

[28] Chatterjee A, Santra M, Won N, Kim S, Kim JK, Kim SB, Ahn KH. Selective fluorogenic and chromogenic probe for detection of silver ions and silver nanoparticles in aqueous media. J Am Chem Soc 2009;131:2040-2041.

[29] Kwon JE, Park SY. Advanced organic optoelectronic materials: harnessing excited-state intramolecular proton transfer (ESIPT) process. Adv Mater 2011;23:3615-3642.

[30] Zhao JZ, Ji SM, Chen YH, Guo HM, Yang P. Excited state intramolecular proton transfer (ESIPT): from principal photophysics to the development of new

chromophores and applications in fluorescent molecular probes and luminescent materials. Phys Chem Chem Phys 2012;14:8803-8817.

[31] Lochbrunner S, Wurzer AJ, Riedle E. Microscopic mechanism of ultrafast excited-state intramolecular proton transfer: A 30-fs study of 2-(2'-hydroxyphenyl)benzothiazole. J Phys Chem A 2003;107:10580-10590.

[32] Abou-Zied OK. Revealing the ionization ability of binding site I of human serum albumin using 2-(2'-hydroxyphenyl)benzoxazole as a pH sensitive probe. Phys Chem Chem Phys 2012;14:2832-2839.

[33] Formosinho SJ, Arnaut LG. Excited-state proton transfer reactions II. Intramolecular reactions. J Photochem Photobiol A Chem 1993;75:21-48.

[34] Paul BK, Guchhait N. Photophysics of a proton transfer phototautomer within biological confinement of a protein: Spectroscopic and molecular docking studies. J Lumin 2014;153:430-438.

[35] Simkovitch R, Shomer S, Gepshtein R, Shabat D, Huppert D. Excited-state proton transfer from quinone-cyanine 9 to protic polar-solvent mixtures. J Phys Chem A 2014;118:1832-1840.

[36] Pal SK, Zewail AH. Dynamics of water in biological recognition. Chem Rev 2004;104:2099-2123.

[37] Santos FS, Ramasamy E, Ramamurthy V, Rodembusch FS. Excited state behavior of benzoxazole derivatives in a confined environment afforded by a water soluble octaacid capsule. J Photochem Photobiol A Chem 2016;317:175-185.

[38] Barbeiro CS, Vasconcelos SNS, Zukerman-Schpector J, Caracelli I, Pimenta DC, Rodrigues ACB, Fernandes AS, Correra TC, Bastos EL, Stefani HA. Chlorinated 2-hydroxynaphthalenoxazolines: synthesis, reaction mechanism and fluorescence properties. ChemistrySelect 2016;1:5647-5652.

[39] Suzuki N, Fukazawa A, Nagura K, Saito S, Kitoh-Nishioka H, Yokogawa D, Irle S, Yamaguchi S. A strap strategy for construction of an excited-state intramolecular proton transfer (ESIPT) system with dual fluorescence. Angew Chem Int Ed 2014;53:8231-8235.

[40] Das K, Sarkar N, Ghosh AK, Majumdar D, Nath DN, Bhattacharyya K. Excited-state intramolecular proton transfer in 2-(2-hydroxyphenyl)benzimidazole and -benzoxazole: effect of rotamerism and

hydrogen bonding. J Phys Chem 1994;98:9126-9132 and references cited therein.

[41] Duarte LGTA, Germino JC, Braga CA, Barboza CA, Atvars TDZ, Santos FS, Rodembusch FS. Photoacidity as a tool to rationalize excited state intramolecular proton transfer reactivity in flavonols. Photochem Photobiol Sci 2018;17:231-238.

[42] Cheknlyuk A, Fadeev V, Georgiev G, Kalkanjiev T, Nickolov Z. Determination of fluorescence quantum yields using a spontaneous Raman scattering line of the solvent as internal standard. Spectrosc Lett 2006;15:355-65.

[43] Frisch MJ, Trucks GW, Schlegel HB, Scuseria GE, Robb MA, Cheeseman JR, G. Scalmani, V. Barone, G. A. Petersson, H. Nakatsuji, X. Li, M. Caricato, A. V. Marenich, J. Bloino, B. G. Janesko, R. Gomperts, B. Mennucci, H. P. Hratchian. Gaussian Inc. 2016.

[44] Chai JD, Head-Gordon M. Long-range corrected hybrid density functionals with damped atom–atom dispersion corrections. Phys Chem Chem Phys 2008;10:6615-6620.

[45] Dunning Jr. TH. Gaussian basis sets for use in correlated molecular calculations. I. The atoms boron through neon and hydrogen. J Chem Phys 1989;90:1007-1023.

[46] Coelho FL, Braga CA, Zanotto GM, Gil ES, Campo LF, Gonçalves PFB, Rodembusch FS, Santos FS. Low pH optical sensor based on benzothiazole azo dyes. Sens Actuators B 2018;259:514-525.

[47] M. Cossi, V. Barone, R. Cammi, J. Tomasi. Ab initio study of solvated molecules: a new implementation of the polarizable continuum model. Chem Phys Lett 1996; 255:327-335.

[48] Andrienko, GA. https://www.chemcraftprog.com

[49] Husain SN, Gentile B, Sauers RR, Eichholz A. Synthesis of photoaffinity labeling derivatives of d-glucose and d-galactose. Carbohyd Res 1983;118:57-63.

[50] Hanessian S, Vakiti RR, Dorich S, Banerjee S, Lecomte F, DelValle JR, Zhang J, Deschênes-Simard B. Total synthesis of pactamycin. Angew Chem Int Ed 2011;50:3497-3500.

[51] Srivastava RM, Neves Filho RA, da Silva CA, Bortoluzzi AJ. First ultrasound-mediated one-pot synthesis of N-substituted amides. Ultrason Sonochem 2009;16:737-742.

[52] Cwik A, Hell Z, Hegedüs A, Finta Z, Horváth Z. A simple synthesis of 2-substituted oxazolines and oxazines. Tetrahedron Lett 2002;43:3985-3987.

[53] Lakowicz JR. Principles of Fluorescence Spectroscopy. 3rd ed. New York: Springer; 2006.

[54] Hansch C, Leo A, Taft RW. A survey of Hammett substituent constants and resonance and field parameters. Chem Rev 1991;91:165-195.

[55] Strickler SJ, Berg RA. Relationship between absorption intensity and fluorescence lifetime of molecules. J Chem Phys 1962;37:814-822.

[56] Turro NJ, Scaiano JC, Ramamurthy V. Principles of Molecular Photochemistry: An Introduction. 1st ed. California: University Science Books; 2008.

[57] Calzaferri G, Rytz R. Electronic transition oscillator strength by the extended Hueckel molecular orbital method. J Phys Chem 1995;99:12141-12150.

[58] Barbara PF, Rentzepis PM, Brus LE. Photochemical kinetics of salicylidenaniline. J Am Chem Soc 1980;102:2786-2791.

[59] Uzhinov BM, Khimich MN. Conformational effects in excited state intramolecular proton transfer of organic compounds. Russ Chem Rev 2011;80:553-577 and references cited therein

[60] Rodembusch FS, Leusin FP, Campo LF, Stefani V. Excited state intramolecular proton transfer in amino 2-(2′-hydroxyphenyl)benzazole derivatives: Effects of the solvent and the amino group position. J Lumin 2007;126:728-734.

[61] Debia NP, Saraiva MT, Martins BS, Beal R, Gonçalves PFB, Rodembusch FS, Lüdtke DS. Synthesis of amino acid-derived 1,2,3-triazoles: development of a non-trivial fluorescent sensor in solution for the enantioselective sensing of a carbohydrate and BSA interaction. J Org Chem 2018;83:1348-1357.

[62] Laurent AD, Jacquemin D. TD-DFT benchmarks: a review. Int J Quantum Chem 2013;113:2019-2039.

[63] Brémond E, Savarese M, Adamo C, Jacquemin D. Accuracy of TD-DFT Geometries: A Fresh Look. J Chem Theory Comput 2018;14:3715-3727.

[64] da Silva CB, Gil ES, Santos FS, Morás AM, Steffens L, Gonçalves PFB, Moura DJ, Lüdtke DS, Rodembusch FS. Proton-transfer-based azides with fluorescence off-on response for detection of hydrogen sulfide: an experimental, theoretical, and bioimaging study. J Org Chem 2018:83;15210-15224.

- ✓ A series of oxazoline derivatives able to proton transfer in the excited state were synthesized
- ✓ Compounds exhibited absorption maxima in the UV region
- ✓ Emission with large Stokes shift (~10000 cm^{-1}) in the blue-green region
- ✓ Optical sensor for enantiomeric identification in solution